Magnetocaloric effect in Heusler alloys $Ni_{50}Mn_{34}In_{16}$ and $Ni_{50}Mn_{34}Sn_{16}$

2007 J. Phys.: Condens. Matter 19 496207

(http://iopscience.iop.org/0953-8984/19/49/496207)

IOP PUBLISHING JOURNAL OF PHYSICS: CONDENSED MATTER

J. Phys.: Condens. Matter **19** (2007) 496207 (12pp) doi:10.1088/0953-8984/19/49/496207

Magnetocaloric effect in Heusler alloys $Ni_{50}Mn_{34}In_{16}$ and $Ni_{50}Mn_{34}Sn_{16}$

V K Sharma[1], M K Chattopadhyay[1], Ravi Kumar[2], Tapas Ganguli[2], Pragya Tiwari[3] and S B Roy[1]

[1] Magnetic and Superconducting Materials Section, Raja Ramanna Centre for Advanced Technology, Indore 452013, India
[2] Semiconductor Laser Section, Raja Ramanna Centre for Advanced Technology, Indore 452013, India
[3] Synchrotron Utilization and Materials Research Division, Raja Ramanna Centre for Advanced Technology, Indore 452013, India

Received 9 July 2007, in final form 16 October 2007
Published 12 November 2007
Online at stacks.iop.org/JPhysCM/19/496207

Abstract

We present results of detailed ac susceptibility, magnetization and specific heat measurements in Heusler alloys $Ni_{50}Mn_{34}In_{16}$ and $Ni_{50}Mn_{34}Sn_{16}$. These alloys undergo a paramagnetic to ferromagnetic transition around 305 K, which is followed by a martensitic transition in the temperature regime around 220 K. Inside the martensite phase both the alloys show signatures of field-induced transition from martensite to austenite phase. Both field- and temperature-induced martensite–austenite transitions are relatively sharp in $Ni_{50}Mn_{34}In_{16}$. We estimate the isothermal magnetic entropy change and adiabatic temperature change across the various phase transitions in these alloys and investigate the possible influence of these transitions on the estimated magnetocaloric effect. The sharp martensitic transition in $Ni_{50}Mn_{34}In_{16}$ gives rise to a comparatively large inverse magnetocaloric effect across this transition. On the other hand the magnitudes of the conventional magnetocaloric effect associated with the paramagnetic to ferromagnetic transition are quite comparable in these alloys.

1. Introduction

Magnetic cooling is drawing worldwide attention due to its potential for more efficient and environmentally friendly refrigeration technology as compared to conventional gas refrigeration [1]. Crucial to the success of magnetic cooling is the availability of materials with large magnetocaloric effect (MCE), which is related to change in magnetic entropy (associated with spin configuration) under application/removal of magnetic field [1]. In materials undergoing first-order magneto-structural transition the structural entropy change also adds to the conventional MCE [2]. In addition, in the systems that undergo a first-order magneto-structural transition with positive temperature coefficient of magnetization, the sign

of isothermal magnetic entropy change (ΔS_M) can be positive in comparison to the negative sign in the conventional MCE [3]. Materials with such inverse MCE find usage as heat sinks for heat generated in refrigeration cycles involving conventional MCE materials [3]. The family of Heusler alloys has been identified to be a potential source of both conventional and inverse MCE. Many alloys belonging to this family undergo a paramagnetic to ferromagnetic transition as a function of temperature, and this transition is then followed by an austenite to martensite phase transition at a lower temperature. Recently we have shown in a $Ni_{50}Mn_{34}In_{16}$ alloy the existence of: (1) a paramagnetic to ferromagnetic transition giving rise to a fairly large conventional MCE in and around room temperature, and (2) a martensitic transition around 220 K accompanying a large inverse MCE [4]. These findings were based entirely on the estimation of ΔS_M from dc magnetization measurements [4]. However, it is now well known that while ΔS_M is a good measure of MCE for a material, the final conclusion on the magnitude of MCE should be based on the estimation of adiabatic temperature change (ΔT_{ad}) under application of an external magnetic field [5]. In this paper we present the results of specific heat measurements on $Ni_{50}Mn_{34}In_{16}$ alloy and estimate ΔT_{ad} for this alloy system from heat capacity data in conjunction with dc magnetization data. Further, we have explored another Heusler alloy system $Ni_{50}Mn_{34}Sn_{16}$ for its potential as an MCE material. Like its indium counterpart, this alloy system also has a paramagnetic to ferromagnetic transition around room temperature, followed by a martensitic transition around 200 K. The MCE associated with the paramagnetic to ferromagnetic transition in this $Ni_{50}Mn_{34}Sn_{16}$ alloy is quite comparable to that of $Ni_{50}Mn_{34}In_{16}$. The inverse MCE accompanying the martensitic transition in $Ni_{50}Mn_{34}Sn_{16}$, however, is considerably smaller than that observed in $Ni_{50}Mn_{34}In_{16}$. The possible reasons for this difference in the magnitude in the inverse MCE in these two quite similar alloy systems will be discussed.

2. Experimental details

The polycrystalline samples of nominal compositions $Ni_{50}Mn_{34}In_{16}$ and $Ni_{50}Mn_{34}Sn_{16}$ were prepared by arc melting the required amount of constituent pure elements under argon gas atmosphere. The samples were flipped and re-melted several times to ensure homogeneity. The samples $Ni_{50}Mn_{34}In_{16}$ and $Ni_{50}Mn_{34}Sn_{16}$ will be denoted as NiMnIn and NiMnSn respectively for further discussion. Samples were cut with a low speed diamond saw and parts of the samples were encapsulated in a quartz glass tube under argon gas for annealing. NiMnIn and NiMnSn samples were annealed at 800 °C for 2 h and 1000 °C for 24 h respectively and then quenched in ice water. Our earlier study on the NiMnIn system was performed on an as-cast sample [4]. Since then we have studied the magnetic and transport properties on an annealed sample of NiMnIn as well. While the character of the paramagnetic to ferromagnetic transition remains the same, the austenite to martensite phase transition is found to be sharper in the annealed sample. However, to be consistent with the results of our earlier measurements, we continued with the as-cast NiMnIn sample in the present study, and this does not influence the general conclusions of the present work. For the NiMnSn system we used an annealed sample. All the samples are characterized with x-ray diffraction (XRD) and energy dispersive x-ray analysis (EDX). This later study determined the actual compositions of NiMnIn and NiMnSn samples to be $Ni_{49.2}Mn_{34.7}In_{16.1}$ and $Ni_{49.8}Mn_{33.5}Sn_{16.7}$ respectively. The ac susceptibility (χ_{ac}) was measured with a homemade mutual inductance type ac susceptometer with an ac magnetic field of amplitude 4 Oe and frequency 333 Hz. The dc magnetization (M) measurements as a function of temperature (T) and magnetic field (H) were performed using a commercial superconducting quantum interface device (SQUID) magnetometer (MPMS-5; Quantum Design) using a scan length of 4 cm with 32 data points in each scan, and a vibrating

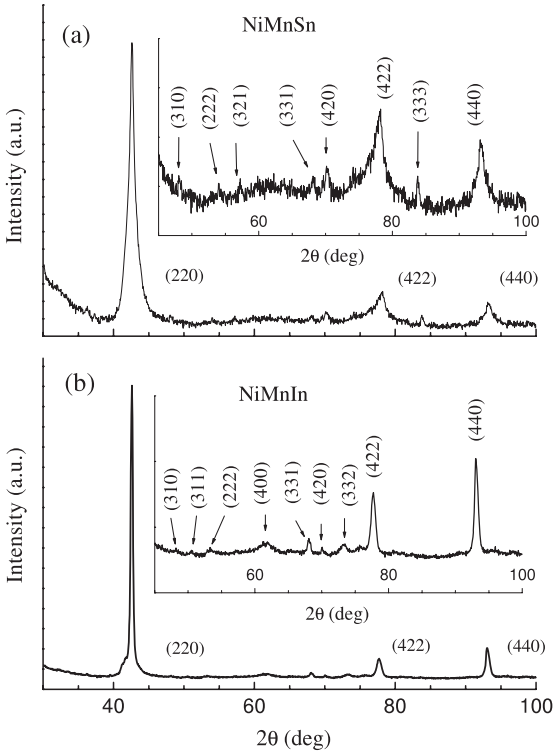

Figure 1. X-ray diffraction patterns of (a) $Ni_{50}Mn_{34}Sn_{16}$ alloy and of (b) $Ni_{50}Mn_{34}In_{16}$ alloys. Only prominent peaks are indexed in the main panels. The insets show details in the range $45° \leqslant 2\theta \leqslant 100°$.

sample magnetometer (VSM, Quantum Design). The heat capacity measurements were made using a commercial thermal properties measurements system (PPMS, Quantum Design).

3. Results and discussion

In this section we shall first present the results of structural and magnetic property measurements in NiMnIn and NiMnSn. We then compare these systems in the perspective of MCE; namely we estimate the isothermal entropy change, adiabatic temperature change and refrigerant capacity for both the systems and compare them. Some of the results on NiMnIn have been reported by us earlier [4] but are reproduced here for the sake of comparison with NiMnSn and to make the present work a self-contained one.

3.1. Structural properties

Figure 1 presents the room temperature XRD patterns of NiMnIn and NiMnSn obtained with Cu Kα radiation. The peaks in the XRD pattern of both the alloys can be indexed to the $L2_1$ structure. Type I superlattice peaks (h, k, l are all odd), which are indicative of the presence of $L2_1$ ordering [6, 7], have been obtained along with the principal peaks (h, k, l are all even and $h + k + l = 4n$). The peaks like (310), (321) and (332) observed in our data are ideally not allowed for stoichiometric composition with the $L2_1$ structure. Their presence can be attributed to the disorder originating from the non-stoichiometry in the samples. XRD peaks of NiMnSn are broader than those of NiMnIn. This probably indicates smaller grain size in the NiMnSn sample. Average lattice constants calculated from prominent peaks are 6.011 and 5.999 Å for

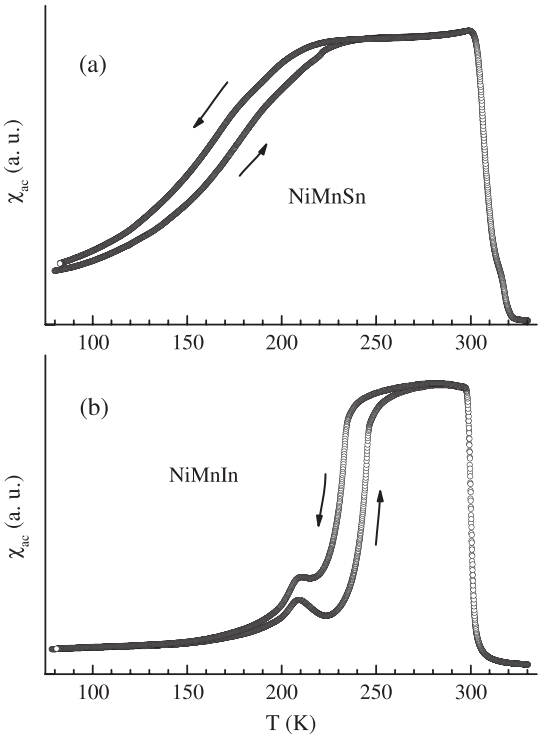

Figure 2. Temperature (T) dependence of ac susceptibility (χ_{ac}) of (a) $Ni_{50}Mn_{34}Sn_{16}$ alloy and of (b) $Ni_{50}Mn_{34}In_{16}$ alloy.

NiMnIn and NiMnSn respectively. These values match closely those reported for the same nominal composition of Ni–Mn–In alloy [8] and nearby composition of Ni–Mn–Sn alloy [9].

3.2. Ac susceptibility

Figure 2 presents a χ_{ac} versus T plot in the T range of 78–330 K for NiMnIn and NiMnSn. In both the alloys there is a sharp rise in χ_{ac} around 305 K with a lowering of T, which is indicative of paramagnetic to ferromagnetic transition in these alloys. The Curie temperatures (T_C) obtained from the point of inflection in the χ_{ac} versus T plots are 305 and 306 K for NiMnIn and NiMnSn respectively. This estimated T_C for NiMnIn agrees well with that obtained from our earlier resistivity and differential scanning calorimetry measurements [10]. There is a subtle shoulder in $\chi_{ac}(T)$ of NiMnSn around T_C (see figure 2). This might arise from a very small amount of magnetic second phase, which has gone undetected in XRD measurements. As T is lowered further, χ_{ac} exhibits an anomalous drop in both the alloys. A distinct thermal hysteresis is associated with this anomalous drop in χ_{ac}. An earlier martensitic transition was reported in the same nominal composition of Ni–Mn–In alloy [8] and nearby composition Ni–Mn–Sn alloy [9] in the same temperature range where this anomalous drop in χ_{ac} is observed. So this effect can be attributed to the martensitic transition in these alloys and accordingly the associated thermal hysteresis is a manifestation of the first-order nature of this transition. The absence of any reversible region in the χ_{ac} versus T (figure 2) plot for NiMnSn in the low T side indicates that the martensitic transition is incomplete up to 78 K in this alloy.

Though both the alloys undergo a martensitic transition around the same T range, χ_{ac} shows significantly different behaviour across the martensitic transition in these alloys. While χ_{ac} decreases over a wider T range in NiMnSn, the change in χ_{ac} is sharp and the hysteresis

extends over a relatively narrow T range in NiMnIn. This is indicative of a broad martensitic transition in NiMnSn. Further, in NiMnIn, χ_{ac} exhibits another feature within the martensitic transition region around 220 K where it shows a local minimum followed by a local maximum with decreasing T. A possible explanation for these features in χ_{ac} is as follows. Martensitic transition involves change in lattice parameters; as a result martensite and austenite phases may have different ferromagnetic characters [3] and the Curie temperatures of the martensite phase (T_{CM}) and of the austenite phase (T_{CA}) may differ. (For a general discussion pertaining to T_{CM}, T_{CA} and the martensitic transition temperature, the readers are referred to [11].) In the present case T_{CA} is the T_C we have estimated from our experiment above. Now if T_{CM} lies within the T regime of martensitic transition, it will lead to a local minimum in the χ_{ac} versus T plot similar to what we have seen in NiMnIn (see figure 2). At the onset of martensitic transition near 240 K in NiMnIn, the martensite phase formed is in the paramagnetic state, so χ_{ac} decreases rapidly with lowering of T. As T is lowered further, there is a paramagnetic to ferromagnetic transition in the martensite phase within the T regime of the martensitic transition and as a result χ_{ac} starts increasing, resulting in a local minimum. Below this paramagnetic to ferromagnetic transition in the martensite phase, χ_{ac} decreases with decreasing T, which is possibly related to the difficulty in the magnetic domain rotation at low temperatures, and so χ_{ac} exhibits a local maximum. T_{CM} lying in the temperature regime of the martensitic transition has been inferred from M data for the same nominal composition of Ni–Mn–In alloy [8]. The absence of such a structure in χ_{ac} in NiMnSn indicates that T_{CM} of this alloy probably does not lie within its martensitic transition region.

3.3. DC magnetization

We have measured the temperature dependence of magnetization for both the NiMnIn and NiMnSn alloys with zero field cooled (ZFC), field cooled cooling (FCC) and field cooled warming (FCW) protocols. However, for the sake of conciseness we present here only the results of FCC and FCW measurements. Figure 3 presents M versus T curves for NiMnIn and NiMnSn in the T range 5–300 K and in various applied fields. We first discuss M–T curves in a magnetic field of 100 Oe (figure 3 bottom panels). At $T = 300$ K NiMnIn and NiMnSn both are in the ferromagnetic phase as $T_C > 300$ K for these alloys. In the case of NiMnIn, with lowering of T there is a rapid fall in M between 240 and 215 K. At 215 K there is a sharp minimum in M, which is followed by an appreciable increase in M with further lowering of T. Also there is a thermal hysteresis in M. The sharp decrease in M around 240 K and thermal hysteresis can be attributed to the martensitic transition occurring in this alloy. It is established that, depending upon the values of T_{CM}, T_{CA} and martensitic transition temperature, the M versus T curve of a ferromagnetic Heusler alloy can exhibit quite different features [11]. The sharp local minimum in M around 215 K followed by a noticeable increase in M with decreasing T have the explanation that T_{CM} lies within the T regime of martensitic transition which we have already inferred from χ_{ac} data. NiMnSn also exhibits a decrease in M with lowering in T around 240 K and a thermal hysteresis, which can be attributed to martensitic transition occurring in this alloy. But M shows no extra feature in the martensitic transition region like that in NiMnIn and the increase in M with decreasing T below the martensitic transition region is relatively small. This finds the explanation that in this alloy T_{CM} is well above the T regime of the martensitic transition. As a result there is no feature in the martensitic transition region and the increase in M with decrease in T in the martensite phase is also small because this T range is far below T_{CM}. This type of relationship between T_{CM} and the martensitic transition temperature regime is reported for a nearby composition of Ni–Mn–Sn alloy [9]. M–T curves in higher field in both the alloys reveal that transition temperatures of the martensitic transition

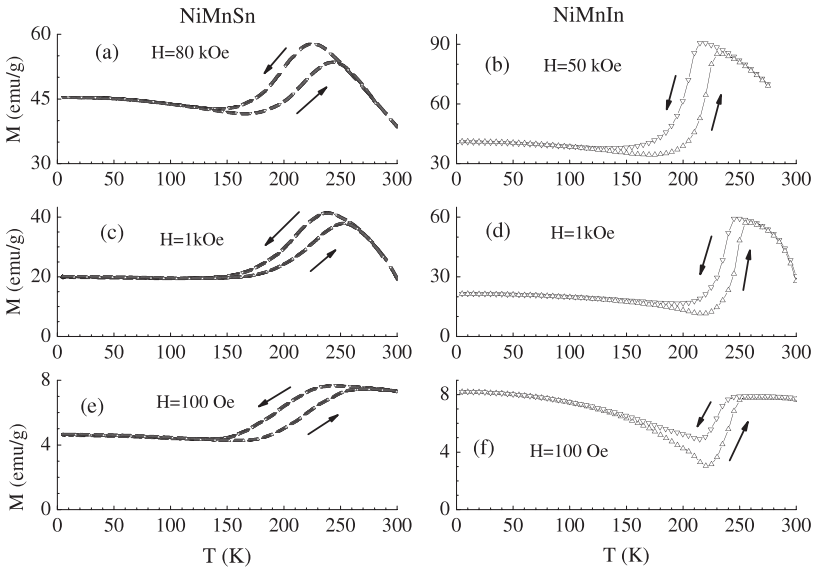

Figure 3. Temperature (T) dependence of magnetization (M) of $Ni_{50}Mn_{34}Sn_{16}$ alloy ((a), (c) and (e)), and of $Ni_{50}Mn_{34}In_{16}$ alloy ((b), (d) and (f)) in various magnetic fields.

shift to the lower T side with increasing H and this shift is much larger in NiMnIn. Also M in the austenite phase has a higher value as compared to that in the martensite phase in both the alloys.

The martensitic transition in both the alloys has the similarity that the martensite phase has a lower value of M than the respective austenite phase, in other words M has positive temperature coefficient across the martensitic transition in both the alloys. The probable reason for the change in spontaneous magnetization can be the change in exchange interaction across the martensitic transition because of different lattice parameters in austenite and martensite phases [3]. It should be noted here that an excess of Mn in these off-stoichiometric alloys with respect to the stoichiometric Ni_2MnIn and Ni_2MnSn, leads to occupation of a number of 4(b) sites in the $L2_1$ structure by Mn atoms [12]. There is an incipient AFM coupling between the magnetic moments of the 4(b) Mn atoms, which can be strengthened further in the martensitic phase [12, 13]. Also characteristic temperatures of martensitic transition shift towards the lower T side with increasing H in both the alloys. On the other hand the martensitic transitions in these alloys are quite different in character. The nature of variation of M across the martensitic transition highlights the basic difference between the martensitic transition in these alloys. It is clear that the transition is rather diffused in NiMnSn. Also the jump in value of M across the martensitic transition is smaller in NiMnSn than in NiMnIn. Furthermore, the shift in transition temperatures of the martensitic transition with H is substantially smaller in NiMnSn, this may be related to the diffused martensitic transition in this alloy. A smaller shift of martensitic transition temperature in Ni–Mn–Sn alloy as compared to that in Ni–Mn–In alloy has been observed for other compositions of these alloy systems [14].

Figure 4 presents isothermal M–H curves up to a maximum field of 80 kOe for NiMnIn and NiMnSn alloys. We have performed M–H measurements at each temperature of interest starting from an initial state, which was prepared by cooling the samples from 300 K to the target temperature in zero field. Then isothermal M–H measurements were performed by changing H from zero to 80 kOe and then back to zero. Figure 4 presents isothermal

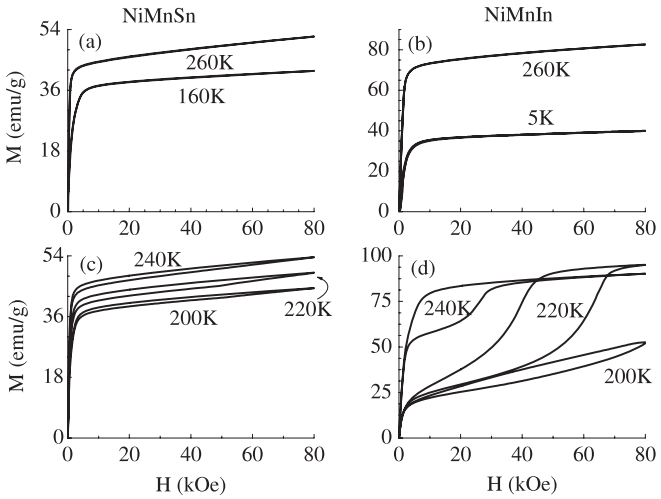

Figure 4. Representative isothermal magnetization (M) versus magnetic field (H) curves of $Ni_{50}Mn_{34}Sn_{16}$ alloy ((a) and (c)) and of $Ni_{50}Mn_{34}In_{16}$ alloy ((b) and (d)) at constant temperatures. M–H curves in the top panels are in the temperature regime well away from martensitic transition region while those in the bottom panels are within the temperature regime of the martensitic transition.

M–H curves at representative temperatures in T regimes well outside the martensitic transition region (top panels) and within the martensitic transition region (bottom panels). Isothermal M–H curves are reversible in the T regime away from the martensitic transition region in both the alloys. This indicates the soft ferromagnetic character of the martensite phase as well as the austenite phase of these alloys. In the crossover regime of austenite to martensitic transition, the isothermal M–H curves exhibit a marked hysteresis. This hysteresis is not related to the ferromagnetic character of martensite and austenite phases but is a result of field-induced first-order transition from martensite to austenite phase. Such hysteresis related to field-induced transition is reported in other magnetic systems [2, 15] and also in Ni–Mn–In [8] and Ni–Mn–Sn [16] alloys. This field-induced transition is much weaker in NiMnSn than in NiMnIn. This substantially different nature of field-induced transition in these quite similar alloys can be correlated to the characteristics of martensitic transitions in these alloys.

3.4. Magnetocaloric effect

Both in NiMnIn and NiMnSn, the magnetization has a positive temperature coefficient across the martensitic transition region. In such systems inverse MCE is expected in the same temperature regime [3]. Furthermore, in NiMnIn there is an appreciable shift of transition temperature along with larger change in M across this transition; so a larger MCE is expected around the martensitic transition in this alloy.

3.4.1. Isothermal entropy change. We have estimated ΔS_M as a function of T at constant H from isothermal M–H curves using the integrated Maxwell's relation [17]

$$\Delta S_M(T)_H = \int_0^H \left[\frac{\partial M(T)}{\partial T}\right]_H \mathrm{d}H. \tag{1}$$

We have measured isothermal M–H curves at discrete intervals of H and T, and ΔS_M was calculated by evaluating the integral in equation (1) with a numerical method [4]. The

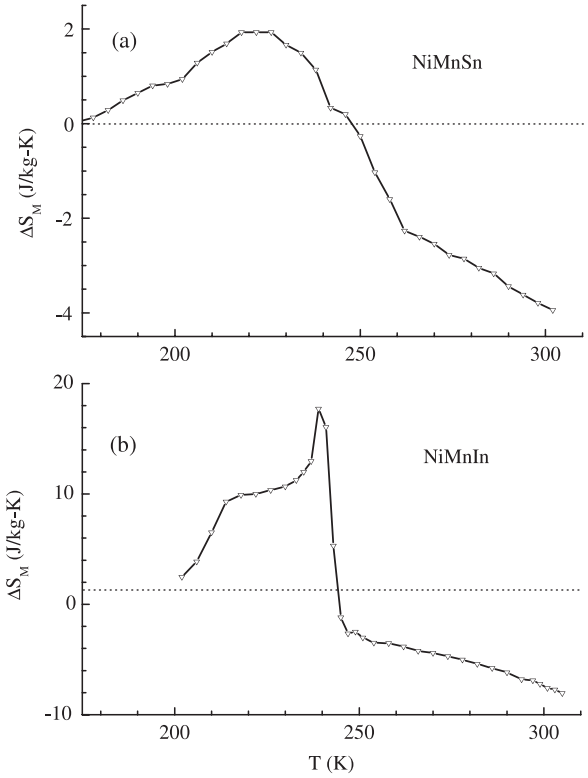

Figure 5. Temperature (T) dependence of isothermal magnetic entropy change (ΔS_M) in (a) $Ni_{50}Mn_{34}Sn_{16}$ alloy and in (b) $Ni_{50}Mn_{34}In_{16}$ alloys for field change of 80 kOe.

temperature dependence of estimated ΔS_M for both the alloys is presented in figure 5 for a maximum field change of 80 kOe. As T increases ΔS_M also increases in both the alloys but the rise in ΔS_M is larger in NiMnIn because of a more prominent field-induced transition in this alloy. In NiMnIn ΔS_M first attains a plateau-like feature and then peaks around 240 K. The presence of such a plateau in ΔS_M is one of the characteristic features of a first-order magnetic transition [18] and is possibly correlated with the field-induced transition in the concerned T range. In NiMnSn magnetic field affects the transition weakly, so in this alloy ΔS_M lacks the plateau-like feature and gradually attains a peak value around 222 K. The T regime of positive ΔS_M in both the alloys corresponds to the respective T regime of the martensitic transition. NiMnSn has a larger T range of positive ΔS_M, which is related to the diffusive character of martensitic transition in this alloy. The peak value of ΔS_M is 19 J kg^{-1} K^{-1} around 240 K for NiMnIn and 2 J kg^{-1} K^{-1} around 220 K for NiMnSn. This peak ΔS_M value for NiMnIn is larger than $\Delta S_M \approx 10$ J kg^{-1} K^{-1} observed in Gd around 295 K [19] but it is considerably smaller in the case of NiMnSn. Furthermore, the maximum ΔS_M obtained for NiMnIn is also greater than that reported for other compositions of Ni–Mn–In alloy systems [13, 20], but the peak value of ΔS_M in NiMnSn is much less than that reported for other compositions of the Ni–Mn–Sn alloy system [3, 21]. These differences, however, are not very surprising as the properties of these alloys are quite sensitive to actual compositions. With further increase in T, ΔS_M changes sign and becomes negative. This is a standard behaviour related to conventional MCE. Near room temperature both the alloys show conventional MCE and the magnitudes of

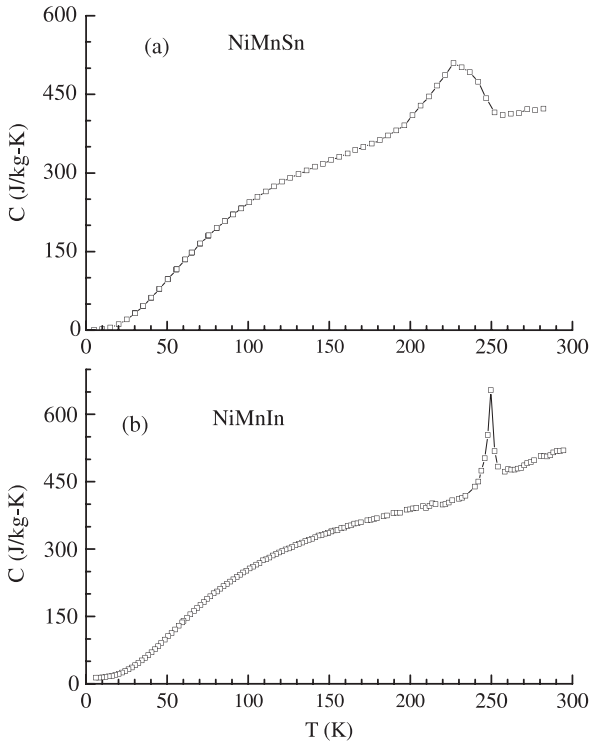

Figure 6. Temperature (T) dependence of heat capacity (C) of (a) $Ni_{50}Mn_{34}Sn_{16}$ alloy and of (b) $Ni_{50}Mn_{34}In_{16}$ alloy in zero magnetic field.

ΔS_M at 300 K are 7.5 and 4 J kg^{-1} K^{-1} for NiMnIn and NiMnSn respectively. These values are quite comparable to that of Gd.

3.4.2. Adiabatic temperature change. Whereas the magnitude of ΔS_M is indicative of the potential of a material for MCE, estimation of the adiabatic temperature change (ΔT_{ad}) is needed for a final conclusion about the magnitude of MCE [5]. We have estimated ΔT_{ad} using the results of heat capacity measurements in conjunction with magnetization data. For an estimation of ΔT_{ad}, the value of entropy (S) as a function of T in zero field and in the field of interest is needed. Zero field S was estimated from heat capacity (C) data measured in zero field. C versus T data in zero field in T range 5–300 K is presented in figure 6 for NiMnIn and NiMnSn. The peaks in $C(T)$ correspond to the martensitic transition in these alloys. NiMnIn shows a sharp peak in C while the peak in C of NiMnSn is much broader. This supports our earlier inference that the martensitic transition in NiMnSn is relatively diffused.

$S(T)$ in zero field as a function of temperature can be calculated using zero field heat capacity data with the following equation [1, 17]

$$S(T)_0 = \int_0^T \frac{C(T)_0}{T}\,\mathrm{d}T + S_0, \tag{2}$$

where $S(T)_0$ and $C(T)_0$ are entropy and heat capacity at temperature T in zero field and S_0 is zero temperature entropy. In a solid-state system S_0 is independent of magnetic field and so can be taken as a constant, say zero [1, 17]. We have estimated S from C data with the numerical method available in the literature [1, 17]. $\Delta S_M(T)_H$ calculated from isothermal magnetization

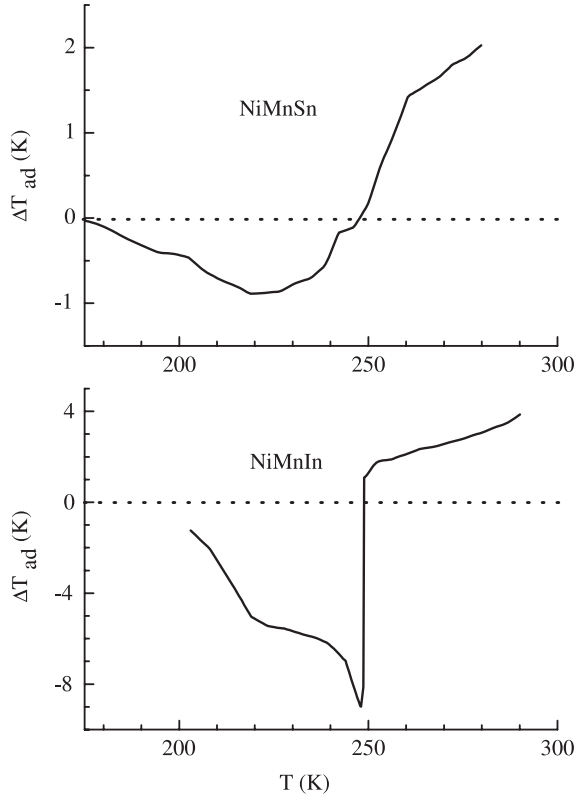

Figure 7. Temperature (T) dependence of the adiabatic temperature change (ΔT_{ad}) for (a) $Ni_{50}Mn_{34}Sn_{16}$ alloy and for (b) $Ni_{50}Mn_{34}In_{16}$ alloys for a field change of 80 kOe.

curves was combined with this zero field entropy to calculate S at constant magnetic field as a function of temperature

$$S(T)_H = S(T)_0 + \Delta S_M(T)_H. \tag{3}$$

From S versus T curves we estimated ΔT_{ad} as a function of temperature. To estimate ΔT_{ad} an iso-entropic path was followed from the zero field S curve to the curve for field H such that $S(T)_0$ equals $S(T + \Delta T_{ad})_H$ and ΔT_{ad} was obtained as [1, 17]

$$\Delta T_{ad}(T)_H = [T(S)_H - T(S)_0]_S. \tag{4}$$

We have estimated ΔT_{ad} for a field change of 80 kOe. Figure 7 presents ΔT_{ad} versus T data for a field change of 80 kOe for both the alloys. As expected, shapes of ΔT_{ad} versus T curves are like inverted ΔS_M versus T curves in both the alloys. A negative ΔT_{ad} corresponding to inverse MCE around the martensitic transition region and a positive ΔT_{ad} corresponding to conventional MCE away from this temperature regime are observed in both the alloys. ΔT_{ad} attains a peak value of -9 K around 248 K in NiMnIn while in the case of NiMnSn the ΔT_{ad} has a peak value of -1 K around 220 K. This magnitude of ΔT_{ad} in NiMnIn is comparable to $\Delta T_{ad} \approx 12$ K reported for Gd [17] and $Gd_5(Si_2Ge_2)$ [22] for a field change of 50 kOe. Furthermore, the magnitudes of ΔT_{ad} are 3 and 2 K at 280 K for a field change of 80 kOe for NiMnIn and NiMnSn respectively.

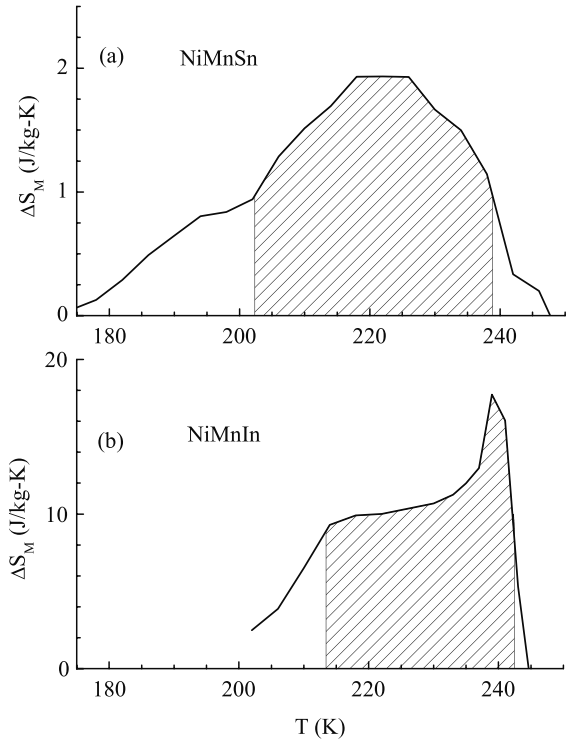

Figure 8. Estimation of refrigerant capacity of (a) $Ni_{50}Mn_{34}Sn_{16}$ alloy and of (b) $Ni_{50}Mn_{34}In_{16}$ alloys for a field change of 80 kOe. Crossed area is measure of RC.

3.4.3. Refrigerant capacity. Refrigerant capacity (RC) is one more parameter of interest in the estimation of MCE. It is a measure of transport of heat between hot and cold reservoirs in an ideal refrigeration cycle [5, 23] and is defined as

$$\mathrm{RC} = \int_{T_1}^{T_2} \Delta S(T)_H \, \mathrm{d}T, \tag{5}$$

where T_1 and T_2 are the temperatures of the cold and hot reservoir of the refrigeration cycle. RC of the refrigerant cycle, in which NiMnIn and NiMnSn are assumed to be the working medium, was calculated using the method available in the literature [5, 23]. In figure 8 the crossed area under the respective ΔS_M versus T curve is a measure of RC of NiMnIn and NiMnSn. The crossed area is calculated by integration over the full width at half maximum. For calculation of effective refrigerant capacity (RC_{EFF}) we first estimated the average hysteresis loss from isothermal M–H curves in the relevant temperature regime and then subtracted it from the calculated RC. RC_{EFF} has a value 220 J kg^{-1} in the case of NiMnIn and 48 J kg^{-1} for NiMnSn for the refrigeration cycle working between the end temperatures of the respective crossed area shown in figure 8. RC_{EFF} in the case of NiMnIn is a bit lower than 305 J kg^{-1} reported for $Gd_5(Si_2Ge_2)$ alloy for a field change of 50 kOe [24], and it is much lower in the case of NiMnSn.

4. Conclusion

Summarizing, we have studied magneto-structural transitions in Heusler alloys $Ni_{50}Mn_{34}Sn_{16}$ and $Ni_{50}Mn_{34}In_{16}$ and their potentials as MCE materials. Both the alloys undergo: (1) a

paramagnetic to ferromagnetic transition near room temperature, (2) a martensitic transition in the temperature regime around 220 K and (3) a field-induced transition from the martensite to austenite phase. The change in magnetization across the martensitic transition is larger in the NiMnIn alloy than in the NiMnSn alloy. This is probably due to the fact that the Curie temperature of the ferromagnetic martensite phase of NiMnIn lies in the same temperature region as the martensitic transition. Furthermore, the field-induced martensite to austenite transition is larger in the NiMnIn alloy than in the NiMnSn alloy. This larger change in magnetization across the martensitic transition and larger field-induced transition in turn give rise to a large inverse magnetocaloric effect in NiMnIn alloy. On the other hand, both the NiMnIn and NiMnSn alloys show appreciable conventional magnetocaloric effect across the paramagnetic to ferromagnetic transition in the austenite phase. The present results suggest that amongst the ferromagnetic Heusler alloys showing a martensitic transition, those particular systems in which the Curie temperature of the martensite phase lies in the same temperature region or below that of the martensitic transition temperature are likely to show a large inverse magnetocaloric effect.

Acknowledgments

The authors acknowledge the help of K H B Shaeb and Parul Arora in ac susceptibility and heat capacity measurements respectively.

References

[1] Tishin A M and Spichkin Y I 2003 *The Magnetocaloric Effect and its Applications* (Bristol: Institute of Physics Publishing)
[2] Pecharsky V K, Holm A P, Gschneidner K A Jr and Rink R 2003 *Phys. Rev. Lett.* **91** 197204
[3] Krenke T, Duman E, Acet M, Wassermann E F, Moya X, Manosa L and Planes A 2005 *Nat. Mater.* **4** 450
[4] Sharma V K, Chattopadhyay M K and Roy S B 2007 *J. Phys. D: Appl. Phys.* **40** 1869
[5] Pecharsky V K and Gschneidner K A Jr 2001 *J. Appl. Phys.* **90** 4614
[6] Webster P J and Ziebeck K R A 1973 *J. Phys. Chem. Solids* **34** 1647
[7] Raphael M P, Ravel B, Huang Q, Willard M A, Cheng S F, Das B N, Stroud R M, Bussmann K M, Claassen J H and Harris V G 2002 *Phys. Rev.* B **66** 104429
[8] Krenke T, Acet M, Wassermann E F, Moya X, Manosa L and Planes A 2006 *Phys. Rev.* B **73** 174413
[9] Krenke T, Acet M, Wassermann E F, Moya X, Manosa L and Planes A 2005 *Phys. Rev.* B **72** 014412
[10] Sharma V K, Chattopadhyay M K, Shaeb K H B, Chouhan A and Roy S B 2006 *Appl. Phys. Lett.* **89** 222509
[11] Chernenko V A, L'vov V A, Zagorodnyuk S P and Takagi T 2003 *Phys. Rev.* B **67** 064407
[12] Brown P J, Gandy A P, Ishida K, Kainuma R, Kanomata T, Neumann K U, Oikawa K, Ouladdiaf B and Ziebeck K R A 2006 *J. Phys.: Condens. Matter* **18** 2249
[13] Krenke T, Duman E, Acet M, Wassermann E F, Moya X, Manosa L, Planes A, Suard E and Ouladdiaf B 2007 *Phys. Rev.* B **75** 104414
[14] Planes A, Manosa L, Moya X, Krenke T, Acet M and Wassermann E F 2007 *J. Magn. Magn. Mater.* **310** 2767
[15] Roy S B, Perkins G K, Chattopadhyay M K, Nigam A K, Sokhey K J S, Chaddah P, Caplin A D and Cohen L F 2004 *Phys. Rev. Lett.* **92** 147203
[16] Koyama K, Watanabe K, Kanomata T, Kainuma R, Oikawa K and Ishida K 2006 *Appl. Phys. Lett.* **88** 132505
[17] Pecharsky V K and Gschneidner K A Jr 1999 *J. Appl. Phys.* **86** 565
[18] Giguere A, Foldeaki M, Gopal B R, Chahine R, Bose T K, Frydman A and Barclay J A 1999 *Phys. Rev. Lett.* **83** 2262
[19] Benford S M and Brown G V 1981 *J. Appl. Phys.* **52** 2110
[20] Han Z D, Wang D H, Zhang C L, Tang S L, Gu B X and Du Y W 2006 *Appl. Phys. Lett.* **89** 182507
[21] Han Z D, Wang D H, Zhang C L, Xuan H C, Gu B X and Du Y W 2007 *Appl. Phys. Lett.* **90** 042507
[22] Pecharsky V K and Gschneidner K A Jr 1999 *J. Appl. Phys.* **86** 6315
[23] Gschneidner K A Jr, Pecharsky V K, Pecharsky A O and Zimm C B 1999 *Mater. Sci. Forum* **315–317** 69
[24] Provenzano V, Shapiro A J and Shull R D 2004 *Nature* **429** 853